Effects of nanocrystalline target and columnar defects on flux pinning in pure and $BaZrO_3$-doped $YBa_2Cu_3O_{6+x}$ films in fields up to 30 T

M. Peurla,[1,2] H. Huhtinen,[1] M. A. Shakhov,[1,3] K. Traito,[1] Yu. P. Stepanov,[1,3] M. Safonchik,[1,3] P. Paturi,[1] Y. Y. Tse,[4] R. Palai,[5] and R. Laiho[1]

[1]*Wihuri Physical Laboratory, Department of Physics, University of Turku, FI-20014 Turku, Finland*

[2]*Graduate School of Materials Research, University of Turku, Turku, Finland*

[3]*A. F. Ioffe Physico-Technical Institute, St. Petersburg 194021, Russia*

[4]*School of Engineering, University of Birmingham, Birmingham B15 2TT, United Kingdom*

[5]*School of Physics and Astronomy, University of Birmingham, Birmingham B15 2TT, United Kingdom*

(Received 1 February 2007; published 24 May 2007)

Transport properties of $YBa_2Cu_3O_{6+x}$ films prepared by pulsed laser deposition from pure and $BaZrO_3$-(BZO-)doped nanocrystalline targets and from a microcrystalline target are investigated in pulsed magnetic fields up to 30 T. As shown by transmission electron microscopy, doping by BZO creates columnar defects of diameter 5–10 nm traversing the films in the direction of the *c* axis. The irreversibility line, the delocalization line, and the high-field critical current density j_c are strongly enhanced in the films deposited from a nanocrystalline target in comparison with those deposited from the microcrystalline target. Doping with BZO further improves the irreversibility and depinning lines and increases the value of j_c. The irreversibility fields of the films prepared from the pure and from the BZO-doped nanocrystalline targets exceed 10 T at 77 K, and at 65 K the value of $j_c \approx 10^5$ A/cm^2 is observed in fields up to 22 T.

DOI: 10.1103/PhysRevB.75.184524 PACS number(s): 74.78.Bz, 74.25.Qt, 74.25.Dw

I. INTRODUCTION

Enhancement of magnetic flux pinning in high-T_c superconductors by inclusions of impurity phase materials is a subject of considerable current interest. In the case of $YBa_2Cu_3O_{6+x}$ (YBCO), various materials such as Y_2BaCuO_5, yttria-stabilized zirconia, $BaZrO_3$ (BZO), etc., have been used to introduce different types of pinning centers into the YBCO lattice. For preparation of thin films by pulsed laser deposition (PLD), ultrathin layers of dopant impurities and YBCO,[1,2] or dopants mixed in the deposition target,[3–7] have been used to create randomly distributed defects and assemblies of columnar structures formed by nanoparticles and nanorods. The average diameter of the columns formed by doping with BZO is between 5 and 10 nm, and their orientation is along the *c* axis of the film, as confirmed by transmission electron microscopy (TEM) and measurements of the angular dependence of the critical current density j_c.[5–7]

It is known that, in comparison with pure YBCO films, the values of j_c can be enhanced by a factor of 2–10 in magnetic fields above 1–3 T, and that some increase of j_c can be observed also in low fields when the films are doped with BZO.[1,5–8] At the same time, also the value of the characteristic field B^*, associated with crossover of the vortex dynamics from single-vortex pinning to the collective pinning regime, is increased.[8] These results have been commonly ascribed to the presence of regular arrays of well-developed columnar defects in the doped films.

We have earlier shown that the value of j_c in a self-field and the plateau of $j_c(B)$ below B^* can be significantly enhanced when the film is laser deposited from a target sintered from YBCO nanopowder instead of the commonly used microcrystalline target.[9–11] This property can be associated with enhanced flux pinning by the specific structure of the film formed when the laser plume contains smaller particles deposited from the nanotarget than those from a microtarget.[12] From structural x-ray diffraction (XRD) and TEM studies,[5,13,16] it has been found that the films made from nanocrystalline material have higher defect density and smaller twin domain size, which leads to faster relaxation of the lattice with the thickness of the films and smaller XRD linewidths.

In this paper, we describe the superconducting properties of YBCO films prepared by PLD from undoped micro- and nanocrystalline YBCO targets and from a nanocrystalline target doped with BZO. The phase diagram of the vortex matter for the investigated films is obtained by current transport measurements in pulsed magnetic fields up to 30 T. While the biggest relative enhancement in the values of $j_c(B)$ is obtained when the film is deposited from the nanocrystalline instead of the microcrystalline target, the superconducting properties of the films in high fields can still be improved by doping with BZO. Also, we present a simple model for how the BZO columns can form from separate particles in the BZO-doped films.

II. EXPERIMENTAL DETAILS

The sample films were prepared by pulsed laser deposition from YBCO targets sintered from pure and optimally doped nanocrystalline powders containing 3.9 wt % BZO.[5] Hereafter these samples will be referred to as *n* films and BZO *n* films, respectively. Details of the preparation of the nanopowders and PLD targets as the well as structures of the obtained *n* films are described elsewhere.[12] For comparison undoped films were also deposited from a conventional YBCO target with micrometer size grains (μ films). The films were deposited on $SrTiO_3$(100) substrates at 790 °C in an atmosphere of 0.3 torr of flowing O_2, and patterned to 35-μm-wide stripes for transport measurements. The thickness of the stripes was between 150 and 200 nm as measured

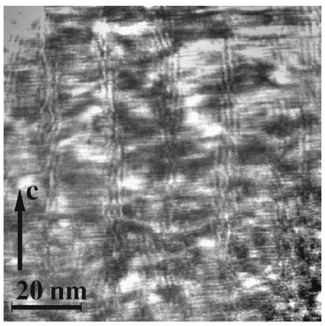

FIG. 1. Cross section TEM image of the BZO *n* film showing columnar defects with width 5–10 nm and spacing ≈20 nm aligned along the *c* axis.

over the stripe edge with an atomic force microscope. The critical temperature of the *n* and μ films was 90 K, and 86 K in the case of the BZO *n* film. Transmission electron microscopy was used for imaging the defects in the *n* films doped with BZO.

The values of j_c in fields up to 6 T were determined from the Bean formula $j_c = 3\Delta M/2R$, where $\Delta M = M_+(B_a) - M_-(B_a)$ is the opening of the magnetic hysteresis loops measured with a superconducting quantum interference device (SQUID) magnetometer and R is the radius of the disk-shaped sample. Transport measurements to determine the $j_c(B)$ dependences in high fields were made in a pulsed magnetic field system with pulse length of 8 ms and fields up to 30 T. During the field pulses, the resistivity of the film, $\rho(B)$, was measured using the four-probe contact method at temperatures between 65 and 89 K and different transport currents up to 50 mA [$\approx(6-10)\times 10^5$ A/cm^2]. The current was applied along the *ab* plane and the magnetic field was parallel to the *c* axis, i.e., perpendicular to the surface of the film. In all resistivity measurements the noise level was $\approx 2 \times 10^{-6}$ Ω cm.

III. INFLUENCE OF BZO NANOPARTICLES ON LOW-FIELD PROPERTIES OF THE FILMS

Figure 1 shows a cross section TEM image of the BZO *n* film, revealing a regular system of prolonged features (Moiré fringes) running along the YBCO *c* axis. The width of these structures, 5–10 nm, and their spacings agree well with the width and distribution of the BZO particles observed earlier in planar view TEM images of the same films.[5] Taking into account the areal surface density of the particles and the thickness of the TEM sample, the volume of the columnar defects calculated from Fig. 1 is roughly twice the amount of BZO in the target material, suggesting that the columns are not completely composed of BZO but contain sections of distorted YBCO in between. This conclusion is consistent with earlier reports,[4] where BZO doping was observed to create self-assembled defects of typical diameter 2–3 nm and spacing 15 nm.

It can be seen from Fig. 1 that the BZO particles are aligned along the *c* axis, showing the anisotropic attraction. One can assume that the elastic stress created by the BZO nanoparticles is important for interpretation of our results. This elastic stress suppresses the conductivity around the BZO nanoparticles, transforming the material into insulator.

To illustrate the formation mechanism of the columnar defects, we consider a unit of two BZO particles separated by a distance R_{min}, corresponding to the minimum of the interaction energy defined by competing contributions of the short-range repulsive and long-range attractive interactions. This model is schematically illustrated in Fig. 2. We assume that the area distorted by the presence of BZO in YBCO has an ellipsoidal shape with the major axis R_c along the crystalline *c* axis and the minor axes R_a along the *a* and *b* axes. The distortion energy of the YBCO structure is proportional to the volume of the hatched area in the figure, VE_{cr}. We assume that the attractive energy density E_{cr} saturates in the distorted area, and this value is taken as the unit of energy. The overlapping volume V from Fig. 2 can be expressed as

$$V = 2\pi y_m^2 R_a^2 \left(1 - \frac{y_m}{3}\right), \quad y_m = 1 - r/2, \tag{1}$$

where r is the distance between BZO quasiparticles, the unit of distance is R_c.

Strong deformation of YBCO is expected when the distance r between the BZO particles is decreased. To limit the number of model parameters we do not take into account the screening of the potential. Therefore, the repulsive potential is modeled as a Coulomb potential CR_c/r instead of a Yukawa potential. The parameter C determines the ratio of the repulsion and attraction energies. The distribution of the two-particle interaction energy in reduced units $C/r - V$ is shown in Fig. 3(b). In this figure we take $C=1$ and $R_c/R_a = 2$. We obtain the value of R_{min} from minimization of the two-particle interaction energy,

$$R_{min} = \sqrt{2\left(1 - \sqrt{1 - \frac{C}{\pi}}\right)}. \tag{2}$$

The calculated distance $R_{min} \approx R_c$ between the BZO particles shown in Fig. 3(a) agrees reasonably with the experimental data, when the filling factor of the BZO particles in the columnar defects is about one-half. In many-particle systems a row of similar minima along the *c* axis is formed, and the BZO particles are placed in the minimum positions, forming a columnar defect.

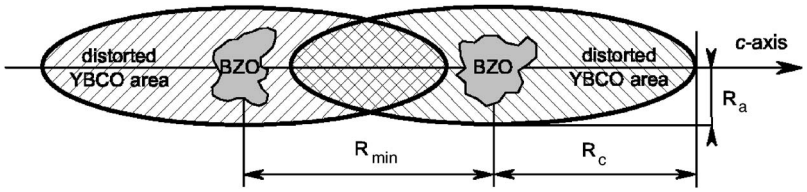

FIG. 2. Schematic representation of the structure of a columnar defect. For R_{min}, R_c, and R_a, see the text.

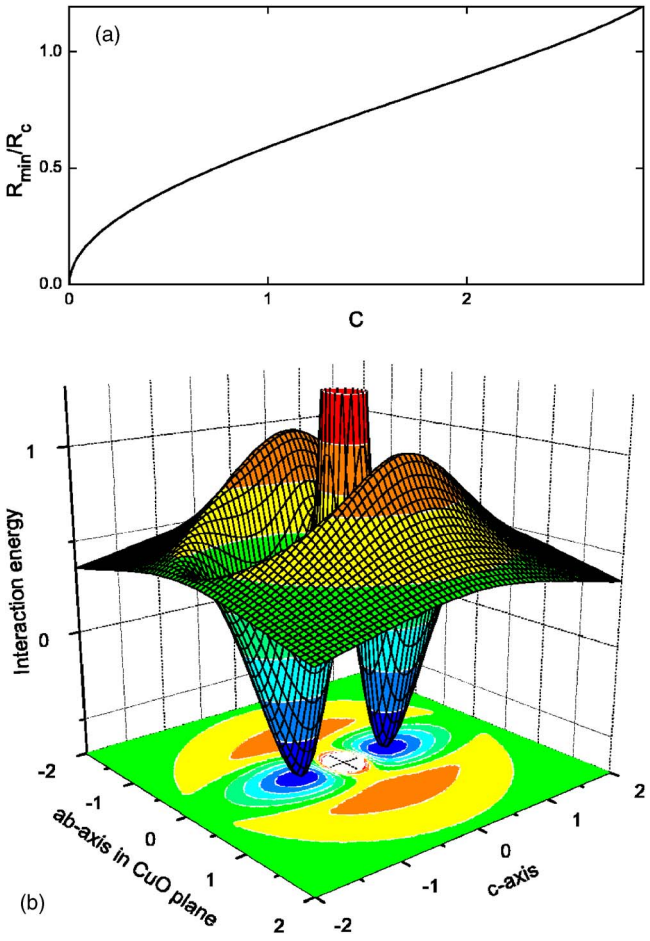

FIG. 3. (Color online) (a) Equilibrium distance between two BZO particles as a function of the ratio C between the repulsive and attractive energies; (b) the dependence of the interaction energy between two particles.

In Fig. 4 are shown the field dependencies of j_c determined at 5 K from the openings of the magnetic hysteresis loops for the three kinds of films. The n film has higher j_c than the μ film. Doping with BZO further improves the value of j_c. The essential parameter in the theoretical model of flux pinning by linear defects is the ratio $x \equiv r_r/\sqrt{2}\xi$ between the radius of the defect, r_r, and the vortex core $\sqrt{2}\xi$.[14] The j_c dependence on the size of a linear defect can be expressed as[15]

$$j_c(T) = \frac{\sqrt{6}}{8x}\left(\frac{2x^2+1}{\sqrt{4x^2+1}} - 1\right) j_0(T), \tag{3}$$

where j_0 is the depairing current. Therefore, for an arbitrary defect size, one can write $j_c = \eta j_0$, where $\eta < 1$ is the efficiency of the pinning center.[15] Generally, in undoped YBCO films, e.g., μ films, the dislocation cores are assumed to be the main pinning centers. Their size is 2–3 nm and the value of η is 0.13.[15] The columnar defects in BZO-doped films are bigger than the dislocation cores, 5–10 nm in diameter, resulting in $\eta \approx 0.25$, which is in perfect agreement with the observed j_c enhancement (Fig. 4). This implies that the n films should have intermediate size columnar defects, $2r_r \approx 4-5$ nm. So far these have not been directly observed, but TEM images have shown[16] that there are "curved" twin planes in the n films, which are missing from the μ films. These could be the reason for the high j_c observed in n films.

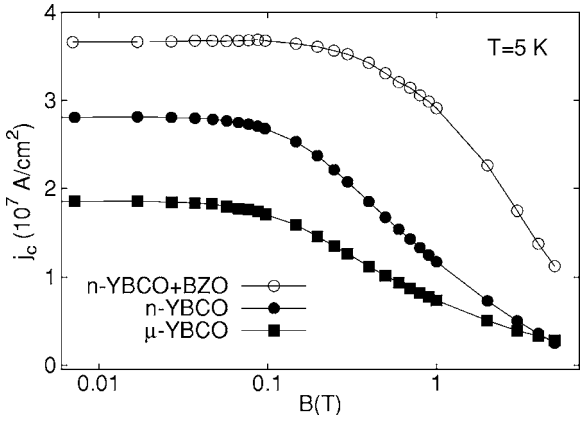

FIG. 4. Field dependencies of j_c at 5 K determined for different sample films from the magnetic hysteresis loops measured with the SQUID magnetometer.

The defect density n_d strongly influences the characteristic field $B^* \sim n_d \Phi_0$ (where Φ_0 is the flux quantum), above which j_c starts to decrease.[5,8] At a high level of n_d the depairing current decreases considerably. This explains the existence of the optimal BZO doping concentration found in Ref. 5.

IV. TRANSPORT MEASUREMENTS IN PULSED FIELDS UP TO 30 T

The field dependences of j_c obtained by pulsed magnetic field experiments are shown in Fig. 5. In agreement with the results obtained in fields below 6 T,[5,8,11] we find the highest j_c in the BZO n film and the lowest in the μ film. The n film and especially the BZO n film have at 65 K values of $j_c = 10^5$ A/cm^2 in fields over 20 T.

Temperature dependences of $\rho(B)$ measured at the probe current of $j \approx 300$ A/cm^2 are shown in Figs. 6(a)–6(c). From these data it is clear that the rise of the resistivity begins in

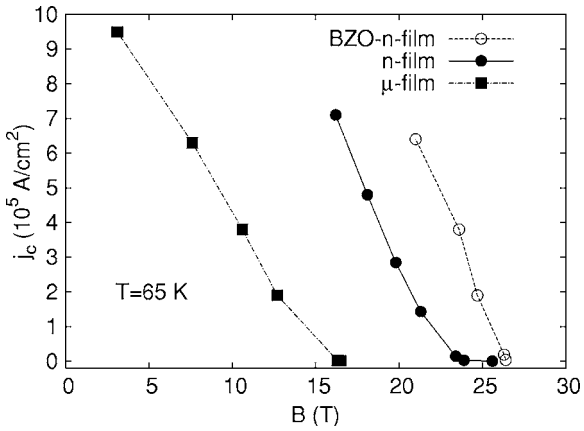

FIG. 5. Critical current densities determined at 65 K using pulsed magnetic fields. The lines are to guide the eye.

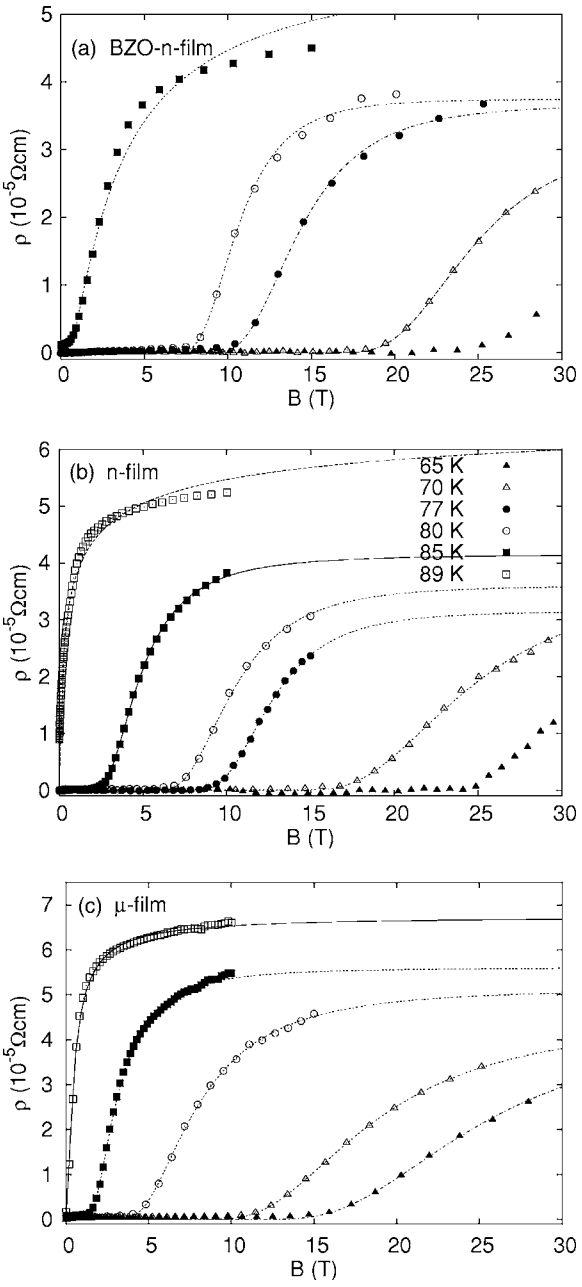

FIG. 6. $\rho(B)$ curves measured at different temperatures for the BZO-doped n film (a), the undoped n film (b), and the undoped μ film (c). The lines are fits to Eq. (4).

much higher fields in the n and the BZO n films than in the μ film. The difference between the n film and the BZO n films is smaller but still well noticeable.

As can be concluded from the temperature dependences of the irreversibility fields B_{irr}, plotted in Fig. 7, the irreversibility line (IRL) of the μ film is located in much lower fields than those of the n film and the BZO n film, the difference being approximately 9 T at 65 K. Because of the lower T_c, the value of B_{irr} in the BZO n film drops strongly above 80 K. In particular, the BZO n film has very high B_{irr} of over 26 T at 65 K and over 10 T at 77 K, higher than those (15–20 T at 65 K and 7–8 T at 77 K) reported for undoped YBCO films.[2,17,18] Recently, values of B_{irr} over 10 T at 77 K

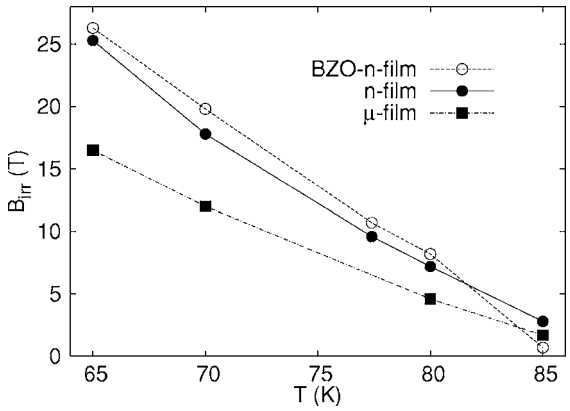

FIG. 7. Temperature dependence of B_{irr} for different films. The lines are to guide the eye.

has been observed in YBCO films doped with Hf.[2] The much closer IRL in the BZO n film and the n film than in the n film and the μ film is similar to what has been observed in irradiated YBCO single crystals, where saturation of the IRL was observed when the density of the columnar defects was increased.[19]

Dependence of the resistivity on temperature and magnetic field is usually expressed in the form $\rho(T,B) \propto e^{-U(B)/T}$, where $U(B) = U_0/B^{\alpha}$ is the field-dependent pinning energy.[20] Therefore the behavior of $\rho(B)$ at constant temperature is given by the equation

$$\rho(B) = \rho_0 e^{-U_0/TB^{\alpha}}, \tag{4}$$

where ρ_0 is the normal state resistivity. Figures 6(a)–6(c) show the fits of the experimental data of $\rho(B)$ with Eq. (4) using ρ_0, U_0, and α as fitting parameters. The fitted ρ_0 and calculated pinning barrier at 20 T and 70 K are listed in Table I. As can be seen, the normal state resistivity is about the same for all the samples, and the pinning energy is about four times higher for the n and BZO n films than for the μ film. These values support the idea that the main difference is between the n film, and the μ film, whereas the BZO doping only brings a slight enhancement in pinning. The irreversibility lines in Fig. 7 also show similar tendencies, being highest in the BZO n film and lowest in the μ film.

The delocalization line $B_{dl}(T)$ separates the vortex nanoliquid from the free flux flow regime or the homogeneous vortex liquid,[21] which persist up to the $B_{c2}(T)$ line. The fields B_{dl} at which $U(B)$ equals the thermal energy were determined from the $U(B)$ plots at different temperatures and are

TABLE I. Fitting parameters from the fits in Fig. 6. ρ_0 is the normal state resistivity and U is the pinning barrier at 20 T and 70 K.

	ρ_0 (10^{-5} Ω cm)	U (20 T, 70 K) (K)
μ film	4.6	39
n film	3.4	124
BZO n film	3.7	189

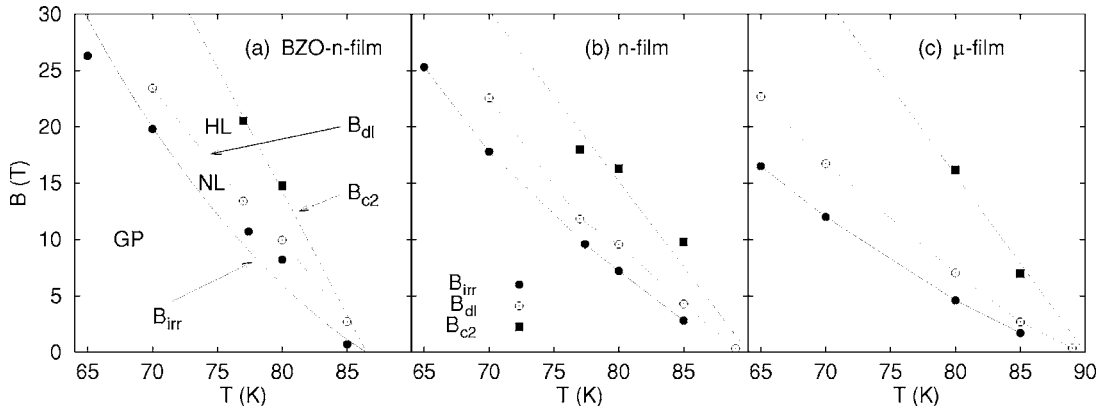

FIG. 8. Phase diagrams of the high-field vortex matter for different films. The solid line in (a) is a fit to Eq. (6). The solid lines in (b) and (c) and the dashed lines are for guiding the eye. GP stands for the vortex glass phase, NL for the vortex nanoliquid, and HL for the homogeneous vortex liquid.

shown in Figs. 8(a)–8(c) for the three films. The plot of $B_{dl}(T)$ defines the delocalization line (DL), above which the flux pinning does not affect the vortex motion and the free flux flow regime is realized. The enhancement of the DL is about 5 T between the μ film and the n film. A further 1–2 T is achieved by doping the n films with BZO. The width of the region between the IRL and DL is nearly the same for all three films. When traced back to the experimental $\rho(B)$ curves in Figs. 6(a)–6(c), the depinning fields correspond to fields around the midpoint (40%–50%) of the transition, where $\rho(B)$ reaches the high-field saturation value.

The end of the transition region of the $\rho(B)$ curves shown in Figs. 8(a)–8(c) by filled squares is interpreted as the second critical field B_{c2}, using the criterion $\rho(B_{c2})/\rho_0=0.9$, where ρ_0 is the normal state resistivity obtained from the fitting for each particular $\rho(B)$ curve. Reliable estimates for B_{c2} were obtained only between 77 and 85 K, where the whole transition region could be measured, resulting in a good fit of $\rho(B)$. Therefore the $B_{c2}(T)$ line was extrapolated using the well-known linear temperature dependence predicted by the Ginzburg-Landau theory at high temperatures. It should be noted that the $B_{c2}(T)$ lines of the investigated films match each other quite well, especially when the lower T_c of the BZO n film is taken into account. This is expected, since the second critical field is not determined by pinning but by the thermodynamics of the equilibrium vortex phase.

Together, the lines $B_{irr}(T)$, $B_{dl}(T)$, and $B_{c2}(T)$ in Fig. 8 define the vortex matter phase diagram. The irreversible vortex phase pinned below IRL melts at the $B_{irr}(T)$ line, forming the vortex nanoliquid.[21] Due to weaker pinning, the irreversible region of the phase diagram, and especially the region of the free flux flow, is largest in the μ film, whereas those of the n and the BZO n films are more similar in size.

In the case of the BZO n film, where the type of defect dominating the pinning is well established, the vortex lattice melting line can be defined by the melting temperatures[14]

$$T_m(B) = T_c\left[1 - \left(\frac{B}{\beta_m c_L^4 H_{c2}(0)/\mathrm{Gi}}\right)^{1/2}\right], \qquad (5)$$

where c_L and Gi are the Lindemann and the Ginzburg numbers, respectively, $H_{c2}(0)$ is the upper critical field at $T=0$ K, and $\beta_m \approx 5.6$. When extended defects like those observed in the BZO n film (Fig. 1) are introduced, the melting line given by Eq. (5) is shifted to[14]

$$T_{irr}(B) \approx \gamma T_m(B) + (1-\gamma)T_c\left(1 - \frac{B}{H_{c2}(0)}\right), \qquad (6)$$

and the effect of the columnar defects can be described by the field-dependent parameter

$$\gamma(B) = \left(1 + \frac{a_0(B) r_r^2}{16 c_L \sqrt{\mathrm{Gi}}\,\xi(0) d_r^2}\right)^{-1}, \qquad (7)$$

where $\xi(0)$ is the coherence length and d_r is the distance between the defects. The magnetic field dependence of the average vortex separation is given by $a_0(B)=\sqrt{\phi_0/B}$. The solid line in Fig. 8(a) shows a fit of the measured IRL of the BZO n film to Eq. (6) using the ratio r_r/d_r as the fitting parameter. For the other parameters we use the values of $c_L=0.15$, $\mathrm{Gi}=10^{-2}$[14], $\xi(0)=2$ nm,[22] and $H_{c2}(0)=120$ T.[18,23] A good fit is obtained with $r_r/d_r=0.32$ in a reasonable agreement with $r_r/d_r \approx 0.25$ calculated using the values of $r_r \approx 5$ nm and $d_r \approx 20$ nm determined from the TEM images.

V. CONCLUSIONS

In conclusion, the flux pinning properties of pure and BZO-doped YBCO films are investigated in pulsed magnetic fields up to 30 T. The upward shifts of the different flux pinning regions of the vortex matter phase diagram indicate enhanced vortex pinning properties in the films prepared by PLD from the nanocrystalline target with respect to those deposited from the microcrystalline target. Further enhancement of j_c is obtained by doping the samples with BZO. TEM images show that the BZO particles create in the film columnar defects of diameter between 5 and 10 nm aligned along the YBCO c axis. A model of these defects agrees with experimentally obtained superconducting properties of the

films. Improved flux pinning and current carrying capacity, especially of the films deposited from the targets made from nanosize powders, enables their use in different high-field applications.

ACKNOWLEDGMENTS

The Wihuri Foundation and the Academy of Finland are acknowledged for financial support.

[1] T. Haugan, P. N. Barnes, R. Wheeler, F. Meisenkothen, and M. Sumption, Nature (London) **430**, 867 (2004).
[2] J. Hänisch, C. Cai, V. Stehr, R. Hühne, J. Lyubina, K. Nenkov, G. Fuchs, L. Schultz, and B. Holzapfel, Supercond. Sci. Technol. **19**, 534 (2006).
[3] J. L. MacManus-Driscoll, S. R. Foltyn, Q. X. Jia, H. Wang, A. Serquis, L. Civale, B. Maiorov, M. E. Hawley, M. P. Maley, and D. E. Peterson, Nat. Mater. **3**, 439 (2004).
[4] A. Goyal, S. Kang, K. J. Leonard, P. M. Martin, A. A. Gapud, M. Varela, M. Paranthaman, A. O. Ijaduola, E. D. Specht, J. R. Thompson, D. K. Christen, S. J. Pennycook, and F. A. List, Supercond. Sci. Technol. **18**, 1533 (2005).
[5] M. Peurla, P. Paturi, Y. P. Stepanov, H. Huhtinen, Y. Y. Tse, A. C. Bódi, J. Raittila, and R. Laiho, Supercond. Sci. Technol. **19**, 767 (2006).
[6] Y. Yamada, K. Takahashi, H. Kobayashi, M. Konishi, T. Watanabe, A. Ibi, T. Muroga, S. Miyata, T. Kato, T. Hirayama, and Y. Shiohara, Appl. Phys. Lett. **87**, 132502 (2005).
[7] C. V. Varanasi, P. N. Barnes, J. Burke, L. Brunke, I. Maartense, T. J. Haugan, E. A. Stinzianni, K. A. Dunn, and P. Haldar, Supercond. Sci. Technol. **19**, L37 (2006).
[8] K. Traito, M. Peurla, H. Huhtinen, Y. P. Stepanov, M. Safonchik, Y. Y. Tse, P. Paturi, and R. Laiho, Phys. Rev. B **73**, 224522 (2006).
[9] H. Huhtinen, P. Paturi, E. Lähderanta, and R. Laiho, Supercond. Sci. Technol. **12**, 81 (1999).
[10] P. Paturi, H. Huhtinen, K. Laajalehto, and R. Laiho, Supercond. Sci. Technol. **13**, 622 (2000).
[11] M. Peurla, H. Huhtinen, and P. Paturi, Supercond. Sci. Technol. **18**, 628 (2005).
[12] H. Huhtinen, J. Järvinen, R. Laiho, P. Paturi, and J. Raittila, J. Appl. Phys. **90**, 1521 (2001).
[13] P. Paturi, M. Peurla, K. Nilsson, and J. Raittila, Supercond. Sci. Technol. **17**, 564 (2004).
[14] G. Blatter, M. Feigel'man, V. Geshkenbein, A. Larkin, and V. Vinokur, Rev. Mod. Phys. **66**, 1125 (1994).
[15] F. C. Klaassen, G. Doornbos, J. M. Huijbregtse, R. C. F. van der Geest, B. Dam, and R. Griessen, Phys. Rev. B **64**, 184523 (2001).
[16] M. Peurla, H. Huhtinen, Y. Y. Tse, J. Raittila, and P. Paturi, IEEE Trans. Appl. Supercond. (to be published).
[17] T. Matsushita, H. Wada, T. Kiss, M. Inoue, Y. Iijima, K. Kakimoto, T. Saitoh, and Y. Shiohara, Physica C **378-381**, 1102 (2002).
[18] H. Nakagawa, T. Takamasu, N. Miura, and Y. Enomoto, Physica B **246-247**, 429 (1998).
[19] A. V. Samoilov, M. V. Feigel'man, M. Konczykowski, and F. Holtzberg, Phys. Rev. Lett. **76**, 2798 (1996).
[20] Y. Z. Zhang, Z. Wang, X. F. Lu, H. H. Wen, J. F. de Marneffe, R. Deltour, A. G. M. Jansen, and P. Wyder, Phys. Rev. B **71**, 052502 (2005).
[21] S. S. Banerjee, S. Goldberg, A. Soibel, Y. Myasoedov, M. Rappaport, E. Zeldov, F. de la Cruz, C. J. van der Beek, M. Konczykowski, T. Tamegai, and V. M. Vinokur, Phys. Rev. Lett. **93**, 097002 (2004).
[22] C. J. van der Beek, M. Konczykowski, A. Abal'oshev, I. Abal'osheva, P. Gierlowski, S. J. Lewandowski, M. V. Indenbom, and S. Barbanera, Phys. Rev. B **66**, 024523 (2002).
[23] T. Sekitani, N. Miura, S. Ikeda, Y. H. Matsuda, and Y. Shiohara, Physica B **346-347**, 319 (2004).